

When do we need to account for the geometric phase in excited state dynamics?

Ilya G. Ryabinkin,^{1,2} Loïc Joubert-Doriol,^{1,2} and Artur F. Izmaylov^{1,2}

¹*Department of Physical and Environmental Sciences, University of Toronto Scarborough, Toronto, Ontario, M1C 1A4, Canada*

²*Chemical Physics Theory Group, Department of Chemistry, University of Toronto, Toronto, Ontario M5S 3H6, Canada*

(Dated: 13 May 2014)

We investigate the role of the geometric phase (GP) in an internal conversion process when the system changes its electronic state by passing through a conical intersection (CI). Local analysis of a two-dimensional linear vibronic coupling (LVC) model Hamiltonian near the CI shows that the role of the GP is twofold. First, it compensates for a repulsion created by the so-called diagonal Born–Oppenheimer correction (DBOC). Second, the GP enhances the non-adiabatic transition probability for a wave-packet part that experiences a central collision with the CI. To assess the significance of both GP contributions we propose two indicators that can be computed from parameters of electronic surfaces and initial conditions. To generalize our analysis to N -dimensional systems we introduce a reduction of a general N -dimensional LVC model to an effective 2D LVC model using a mode transformation that preserves short-time dynamics of the original N -dimensional model. Using examples of the bis(methylene) adamantyl and butatriene cations, and the pyrazine molecule we have demonstrated that their effective 2D models reproduce the short-time dynamics of the corresponding full dimensional models, and the introduced indicators are very reliable in assessing GP effects.

I. INTRODUCTION

Conical intersections (CIs) of electronic states provide an efficient mechanism for radiationless electronic transitions.^{1–3} CIs act as “funnels”⁴ for the nuclear density and enables rapid conversion of the excessive electronic energy into nuclear motion. Owing to the ubiquity of CIs in molecules,^{3,5–16} an adequate theoretical description of this conversion mechanism is an important task in theoretical physical chemistry.

Conical intersections of potential energy surfaces lead not only to non-adiabatic transitions but also to the appearance of the geometric phase (GP)^{17–19} in both electronic and nuclear wave-functions. The GP manifests in a sign change of adiabatic electronic wave-functions along a closed path of nuclear configurations encircling the CI seam.^{18,20} This sign change must be compensated by corresponding nuclear wave-functions in order to preserve the single-valued character of the total wave-function. The GP poses a challenge for modelling non-adiabatic dynamics because nuclear wave-functions must be simulated with double value boundary conditions (DVBC). Neglecting DVBC for low energy nuclear dynamics on the ground electronic state near the CI can result in qualitatively wrong predictions.^{21,22} The GP causes an extra phase accumulation for fragments of the nuclear wave-packet that skirt the CI on opposite sides.^{23,24} Resulting destructive interference can lead either to a spontaneous localization of the nuclear density²⁴ or slower nuclear dynamics²⁵ than in the case where the GP is neglected.

A question arises about the role of the GP in the excited state nuclear dynamics through the CI. Recently, Althorpe and co-workers put forward a topological analysis considering Feynman path integral trajectories and their “winding numbers”.^{26–28} Practically, for photo-

induced interconversion processes this analysis involves numerical simulation of quantum nuclear wave-packet dynamics with and without GP-induced DVBC and evaluation of wave-packet components that are even and odd with respect to the 2π rotation around the CI. The spatial overlap between the even and odd components provides a measure of GP significance. The obvious difficulty with this analysis is a necessity of quantum dynamics with and without GP-induced DVBC, such simulations cannot be easily done for a general molecular system.

Recent studies^{28,29} of non-adiabatic transitions in photodissociation of pyrrole have shown that the impact of the GP on the dynamics near ${}^1B_1 - S_0$ and ${}^1A_2 - S_0$ CIs is quite different. For ${}^1B_1 - S_0$ it changed the branching ratio between two fragmentation products only slightly, while for ${}^1A_2 - S_0$ stronger GP effects were found. To date, no satisfactory explanation of this difference has been given. On the other hand, several research groups are actively develop on-the-fly non-adiabatic dynamics techniques following mixed quantum-classical approach that neglects GP effects. It is not clear how results of these techniques would change if GP effects were included. Thus, it is highly desirable to build a theory that can predict the significance of the GP without performing full dimensional quantum nuclear dynamics simulations.

To address this challenge we begin our consideration with analysis of one of the simplest two-dimensional diabatic models that can provide the CI in the adiabatic representation.^{20,30–32} In the 2D model we demonstrate that for excited state dynamics mostly local properties in a vicinity of the CI define significance of the GP, and a great body of system-specific information on a periphery of the CI is secondary. Considering an N -dimensional extension of our model we propose a transformation that reduces the system dimensionality back to two while pre-

serving short-time dynamics of the N -dimensional case. Using this reduction transformation we extend the 2D analysis to N -dimensional models. Finally, from the local analysis we devise characteristics that can be obtained from electronic structure calculations for molecules and can predict significance of GP effects for molecular non-adiabatic dynamics.

Note that the GP appears only in the adiabatic representation because it is a property of adiabatic electronic and nuclear wave-functions. In the diabatic representation^{33–35} the GP is absent. Still, due to equivalence of the diabatic and adiabatic representations, dynamical features that appear only when the GP is included in the adiabatic representation are present in the diabatic dynamics but constitute its indiscernible from other effects part. Thus, due to absence of the GP in the diabatic representation, it is easier numerically to perform exact dynamics in that representation. The main problem with the diabatic representation is that it cannot be rigorously defined for a finite number of electronic states in a general molecular system.^{34,35} The adiabatic representation is a primary representation available from the first-principles (*ab initio*) calculations for molecules, and the diabatic representation is usually obtained from the adiabatic representation in some approximate way.^{13,36–39} However, since the reversed transformation from the diabatic to the adiabatic representation is always exact, we use diabatic models and the associated adiabatic representation to analyze GP effects.

This paper is organized as follows. First, by analyzing the difference between model Hamiltonians with and without account for the GP we identify two main GP effects that modify non-adiabatic dynamics. Second, we discuss two indicators that allow us to assess the importance of GP effects without simulating quantum dynamics. Third, we simulate and analyze non-adiabatic dynamics for a few molecular systems that provide a variety of dynamical regimes and allows us to probe limitations of our theoretical analysis. Finally, we conclude the paper with a summary and an outlook for future work. Atomic units are used throughout this paper.

II. THEORETICAL ANALYSIS

A. Two-dimensional linear vibronic coupling model

We begin our consideration of the two-dimensional linear vibronic coupling (LVC) model with its Hamiltonian

$$\hat{H} = \hat{T}\mathbf{1}_2 + \begin{pmatrix} V_{11} & V_{12} \\ V_{12} & V_{22} \end{pmatrix}, \quad (1)$$

where $\hat{T} = -\frac{1}{2}\nabla^2 \equiv -\frac{1}{2}(\partial^2/\partial x^2 + \partial^2/\partial y^2)$ is the nuclear kinetic energy operator, and $\mathbf{1}_2$ is a 2×2 unit matrix. V_{11} and V_{22} are the diabatic potentials represented by identical 2D parabolas shifted in the x -direction by a , in

energy by Δ

$$V_{11} = \frac{\omega_1^2}{2} \left(x + \frac{a}{2}\right)^2 + \frac{\omega_2^2}{2} y^2 + \frac{\Delta}{2}, \quad (2)$$

$$V_{22} = \frac{\omega_1^2}{2} \left(x - \frac{a}{2}\right)^2 + \frac{\omega_2^2}{2} y^2 - \frac{\Delta}{2}. \quad (3)$$

To have the CI in the adiabatic representation V_{11} and V_{22} are coupled by the linear $V_{12} = cy$ potential. Switching to the adiabatic representation for the 2D LVC Hamiltonian in Eq. (1) is done by diagonalizing the potential matrix using a unitary transformation

$$U = \begin{pmatrix} \cos \theta & \sin \theta \\ -\sin \theta & \cos \theta \end{pmatrix}, \quad (4)$$

where θ is a mixing angle between the diabatic electronic states $|1\rangle$ and $|2\rangle$

$$\theta = \frac{1}{2} \arctan \frac{2V_{12}}{V_{11} - V_{22}} = \frac{1}{2} \arctan \frac{\gamma y}{x + b}. \quad (5)$$

Here, $b = \Delta/(\omega_1^2 a)$ is the x -coordinate of the CI point, and $\gamma = 2c/(\omega_1^2 a)$ is dimensionless coupling strength. For simplicity of the subsequent analysis we set $b = 0$, which corresponds to centering the coordinates at the CI point.

The transformation in Eq. (4) gives rise to the 2D LVC Hamiltonian in the adiabatic representation $\hat{H}_{\text{adi}} = U\hat{H}U^\dagger$,

$$\hat{H}_{\text{adi}} = \begin{pmatrix} \hat{T} + \hat{\tau}_{11} & i\hat{\tau}_{12} \\ -i\hat{\tau}_{21} & \hat{T} + \hat{\tau}_{22} \end{pmatrix} + \begin{pmatrix} W_- & 0 \\ 0 & W_+ \end{pmatrix}, \quad (6)$$

where

$$W_\pm = \frac{1}{2}(V_{11} + V_{22}) \pm \frac{1}{2}\sqrt{(V_{11} - V_{22})^2 + 4V_{12}^2}, \quad (7)$$

are the adiabatic potentials and $\hat{\tau}_{ij}$ are the non-adiabatic couplings. For our model we can further express $\hat{\tau}_{ij}$ as

$$\hat{\tau}_{11} = \hat{\tau}_{22} = \frac{1}{2}\nabla\theta \cdot \nabla\theta = \frac{x^2 + y^2}{8(\gamma^{-1}x^2 + \gamma y^2)^2}, \quad (8)$$

$$\begin{aligned} \hat{\tau}_{12} = \hat{\tau}_{21} &= \frac{i}{2} \left(\overleftarrow{\nabla} \cdot \nabla\theta - \nabla\theta \cdot \overrightarrow{\nabla} \right) \\ &= \frac{(\overleftarrow{L}_z - \overrightarrow{L}_z)}{4(\gamma^{-1}x^2 + \gamma y^2)}, \end{aligned} \quad (9)$$

where $L_z = xp_y - yp_x$ is the z component of the angular momentum operator, and the overhead arrows indicate the directions in which the differential operators act.⁴⁰ The diagonal non-adiabatic couplings, $\hat{\tau}_{11}$ and $\hat{\tau}_{22}$, represent a repulsive potential known as the diagonal Born–Oppenheimer correction (DBOC).^{41,42} The DBOC is the parametric function of the coupling strength parameter γ . Figure 1 illustrates the DBOC for representative values of γ . The off-diagonal elements, $\hat{\tau}_{12}$ and $\hat{\tau}_{21}$ in Eq. (9), couple dynamics on the adiabatic potentials W_\pm and are responsible for non-adiabatic transitions.

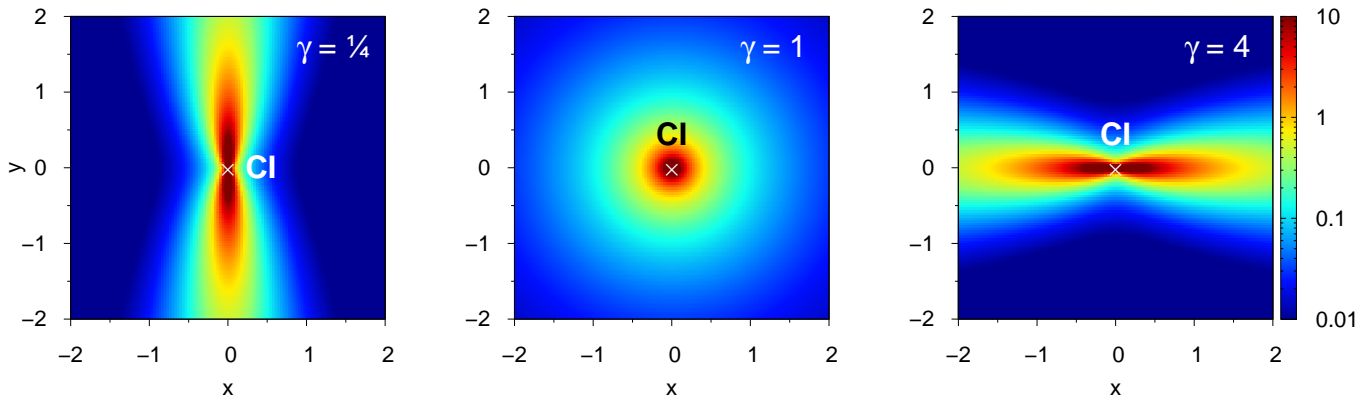


FIG. 1. The diagonal Born-Oppenheimer correction, Eq. (8), for different values of γ .

If we simulate the spectrum or nuclear dynamics for \hat{H}_{adi} using single-valued basis functions, the outcome can be very different from that for the original full Hamiltonian \hat{H} .²⁴ This difference arises as a result of ignoring proper DVBC for the \hat{H}_{adi} Hamiltonian. The unitary transformation U changes its sign if one encircles the CI point using the parametric dependence of θ on the nuclear coordinates x and y . Since the adiabatic electronic states are columns of the U matrix in the diabatic basis, this sign change is a manifestation of the GP that is acquired by the adiabatic electronic wave-functions.^{17–19} The total electron-nuclear wave-function is always single-valued and thus DVBC for the electronic part impose the DVBC for the corresponding nuclear part. As a consequence, to simulate the nuclear dynamics of \hat{H}_{adi} with a proper account of GP effects, one needs to impose DVBC. To assess the importance of GP effects we use simulations of the \hat{H}_{adi} non-adiabatic dynamics *without* imposing DVBC as a reference which will be referred to as the “no GP” model.

To account for GP effects in the adiabatic representation we follow the Mead and Truhlar¹⁸ technique that introduces a position-dependent phase factor $e^{i\theta}$ with θ given by Eq. (5). This phase factor changes the sign upon encircling the CI and can be either attached to nuclear basis functions to introduce DVBC or alternatively used to transform \hat{H}_{adi} into $\hat{H}_{\text{GP}} = e^{-i\theta} \hat{H}_{\text{adi}} e^{i\theta}$. We will follow the second path because GP effects in the \hat{H}_{GP} Hamiltonian have a concrete operator representation that will facilitate our analysis. Since the $e^{i\theta}$ transformation of \hat{H}_{adi} contains only functions of nuclear coordinates, \hat{H}_{GP} is different from \hat{H}_{adi} only in the kinetic energy part

$$\hat{H}_{\text{GP}} = \begin{pmatrix} \hat{T} + \hat{\tau}_{11}^{\text{GP}} & i\hat{\tau}_{12}^{\text{GP}} \\ -i\hat{\tau}_{21}^{\text{GP}} & \hat{T} + \hat{\tau}_{22}^{\text{GP}} \end{pmatrix} + \begin{pmatrix} W_- & 0 \\ 0 & W_+ \end{pmatrix}, \quad (10)$$

where

$$\begin{aligned} \hat{\tau}_{11}^{\text{GP}} &= \hat{\tau}_{22}^{\text{GP}} = \hat{\tau}_{11} + \left(e^{-i\theta} \hat{T} e^{i\theta} - \hat{T} \right) \\ &= \hat{\tau}_{11} + \frac{i}{2} \left(\overleftarrow{\nabla} \cdot \nabla \theta - \nabla \theta \cdot \overrightarrow{\nabla} \right) + \frac{1}{2} \nabla \theta \cdot \nabla \theta \\ &= \frac{(\overrightarrow{L}_z - \overleftarrow{L}_z)}{4(\gamma^{-1}x^2 + \gamma y^2)} + \frac{x^2 + y^2}{4(\gamma^{-1}x^2 + \gamma y^2)^2}, \end{aligned} \quad (11)$$

$$\begin{aligned} \hat{\tau}_{12}^{\text{GP}} &= \hat{\tau}_{21}^{\text{GP}} = e^{-i\theta} \hat{\tau}_{12} e^{i\theta} \\ &= \frac{(\overrightarrow{L}_z - \overleftarrow{L}_z)}{4(\gamma^{-1}x^2 + \gamma y^2)} - \frac{x^2 + y^2}{4(\gamma^{-1}x^2 + \gamma y^2)^2}. \end{aligned} \quad (12)$$

Comparison of Eqs. (11)–(12) with Eqs. (8)–(9) shows that the GP modifies the non-adiabatic coupling matrix elements and thus changes probabilities of non-adiabatic transitions.

B. The role of the geometric phase in non-adiabatic transitions

Below we further separate individual physical mechanisms that stem from the mathematical differences in $\hat{\tau}$ operators for models with and without the GP.

1. Compensation of the DBOC repulsion

The non-adiabatic couplings $\hat{\tau}_{ij}$ and $\hat{\tau}_{ij}^{\text{GP}}$ are singular at the CI, therefore we can neglect any regular operator in a vicinity of the CI. In particular, the difference of the adiabatic potentials is not only a regular operator but also vanishes at the CI [$W_+(\mathbf{r}_{\text{CI}}) = W_-(\mathbf{r}_{\text{CI}})$]. This allows us to consider the kinetic matrix in Eq. (6) alone. Applying a unitary rotation in the electronic subspace

we can diagonalize the kinetic matrix

$$\frac{1}{2} \begin{pmatrix} 1 & i \\ 1 & -i \end{pmatrix} \begin{pmatrix} \hat{T} + \hat{\tau}_{11} & i\hat{\tau}_{12} \\ -i\hat{\tau}_{21} & \hat{T} + \hat{\tau}_{22} \end{pmatrix} \begin{pmatrix} 1 & 1 \\ -i & i \end{pmatrix} \quad (13)$$

$$= \begin{pmatrix} \hat{T} + \hat{\tau}_- & 0 \\ 0 & \hat{T} + \hat{\tau}_+ \end{pmatrix},$$

where $\hat{\tau}_\pm = \hat{\tau}_{11} \pm \hat{\tau}_{12}$ (note that $\hat{\tau}_{11} = \hat{\tau}_{22}$ and $\hat{\tau}_{12} = \hat{\tau}_{21}$). Eigenstates of decoupled sub problems

$$(\hat{T} + \hat{\tau}_\pm)\chi_n^\pm = \epsilon_i^\pm \chi_i^\pm, \quad i = 1, \dots \quad (14)$$

represent a convenient complete set of functions to expand any wave-function in a vicinity of the CI. However, properties of the eigenstates χ_i^\pm are quite different for the models with and without the GP. Using Eqs. (8) and (9), we can write $\hat{\tau}_\pm$ for the “no GP” case as

$$\hat{\tau}_\pm = \frac{(x^2 + y^2) \pm (\vec{L}_z - \overleftarrow{L}_z)}{8(\gamma^{-1}x^2 + \gamma y^2)^2}, \quad (15)$$

where both coupling and DBOC terms are intermixed. The singular DBOC term gives rise to a cusp behavior at the CI point for the eigenstates χ_i^\pm to maintain finite energy. A cusp-less wave-packet of finite energy cannot reach the CI, since any finite-energy expansion in terms of the eigenstates χ_i^\pm must have a node at the CI. In contrast, with the GP [Eqs. (11) and (12)] we have

$$\hat{\tau}_+^{\text{GP}} = \frac{\vec{L}_z - \overleftarrow{L}_z}{2(\gamma^{-1}x^2 + \gamma y^2)^2}, \quad (16)$$

$$\hat{\tau}_-^{\text{GP}} = \frac{x^2 + y^2}{2(\gamma^{-1}x^2 + \gamma y^2)^2}, \quad (17)$$

where there is a clear separation on the operator term $\hat{\tau}_+^{\text{GP}}$ and the scaled DBOC term $\hat{\tau}_-^{\text{GP}}$. Since $\hat{\tau}_+^{\text{GP}}$ does not contain the DBOC, functions that satisfy $L_z \chi_i^+ = 0$ form a suitable subset of the eigenstates which can be *finite* at the CI. Therefore, in the presence of the GP a cusp-less wave-packet can access the CI point.

Interpreting the DBOC as physical repulsion, we can say that this repulsion does not allow a wave-packet to reach the CI in the “no GP” case, whereas in the presence of the GP this repulsion is *compensated* and the wave-packet can reach the CI. This compensation is especially important in the small coupling case, $\gamma \ll 1$ (see Fig. 1 $\gamma = 1/4$), because the DBOC represents a repulsive wall that can block all parts of an incoming wave-packet from accessing regions where the off-diagonal couplings, Eq. (9), are large. If $\gamma \approx 1$ (see Fig. 1 $\gamma = 1$), the DBOC repulsion and its GP compensation become less important because only a central part of the wave-packet is significantly repelled while peripheral parts can reach large coupling areas.

The idea of compensation of the DBOC repulsion by the GP can be further explored by introducing a simplified “no GP, no DBOC” Hamiltonian without the diag-

onal non-adiabatic terms $\hat{\tau}_{ii}$

$$\hat{H}_{\text{adi}}^{(s)} = \begin{pmatrix} \hat{T} & i\hat{\tau}_{12} \\ -i\hat{\tau}_{21} & \hat{T} \end{pmatrix} + \begin{pmatrix} W_- & 0 \\ 0 & W_+ \end{pmatrix}. \quad (18)$$

If the compensation mechanism is significant, the dynamics produced by $\hat{H}_{\text{adi}}^{(s)}$ will be closer to that of the full Hamiltonian [Eq. (1)] than to the “no GP” Hamiltonian [Eq. (6)].

2. Non-adiabatic transfer enhancement

The non-adiabatic couplings $\hat{\tau}_{ij}$ in models with or without the GP contain the z -component of the angular momentum operator L_z [see Eqs. (9) and (12)]. Although the 2D LVC has cylindrical symmetry only when $\gamma = 1$ (see Fig. 1), the presence of L_z suggests to analyze dynamics of a wave-packet ψ by expanding it in the eigenstates of L_z

$$\psi(x, y, t) = \sum_{m=-\infty}^{\infty} C_m(r, t) e^{-im\phi}, \quad (19)$$

where r and ϕ are the polar coordinates centered at the CI. Action of the coupling on ψ can be analyzed starting from the L_z operator

$$L_z \psi(x, y, t) = \sum_{m=-\infty}^{\infty} m C_m(r, t) e^{-im\phi}. \quad (20)$$

Considering non-adiabatic transition for the $m = 0$ component of ψ we have

$$\hat{\tau}_{12} C_0(r, t) = \frac{(\vec{L}_z - \overleftarrow{L}_z)}{4(\gamma^{-1}x^2 + \gamma y^2)} C_0(r, t) \quad (21)$$

$$= \frac{-\overleftarrow{L}_z C_0(r, t)}{4(\gamma^{-1}x^2 + \gamma y^2)}. \quad (22)$$

Introducing a resolution of the identity in the angular coordinate

$$\mathbf{1}_\phi = \frac{1}{2\pi} \int_0^{2\pi} d\phi \sum_{m'=-\infty}^{+\infty} e^{im'(\phi' - \phi)} \quad (23)$$

into Eq. (22) we obtain

$$\begin{aligned} \hat{\tau}_{12} C_0(r, t) &= \frac{1}{2\pi} \int_0^{2\pi} d\phi \sum_{m'=-\infty}^{+\infty} e^{im'(\phi' - \phi)} \\ &\times \frac{-\overleftarrow{L}_z C_0(r, t)}{4(\gamma^{-1}x^2 + \gamma y^2)} \quad (24) \\ &= \frac{1}{2\pi} \sum_{m'=-\infty}^{+\infty} e^{im'\phi'} m' C_0(r, t) \\ &\times \int_0^{2\pi} \frac{e^{-im'\phi} d\phi}{4[\gamma r^2 + (\gamma^{-1} - \gamma)r^2 \cos^2 \phi]}. \quad (25) \end{aligned}$$

If $\gamma = 1$, the angular integral in Eq. (25) becomes zero and there is no transfer for the $m = 0$ component in the cylindrical symmetric case. For $\gamma \neq 1$, the angular integral in Eq. (25) is non-zero, and only $m' \neq 0$ contributions survive in the sum over m' . Therefore, even if cylindrical symmetry is broken, $\hat{\tau}_{12}$ can transfer the $m = 0$ component only to the $m' \neq 0$ components. Due to an increase in kinetic energy associated with this process, the transfer probability is reduced compared to that for the $m \neq 0$ components of the initial wave-packet.

For the model with GP, $\hat{\tau}_{12}^{\text{GP}}$ in Eq. (12) contains the L_z -independent contribution. Thus, when $\gamma \neq 1$ the $m = 0$ component can be transferred into both $m' \neq 0$ and $m' = 0$ components

$$\begin{aligned} \hat{\tau}_{12}^{\text{GP}} C_0(r, t) &= \frac{-\overleftarrow{L}_z C_0(r, t)}{4(\gamma^{-1}x^2 + \gamma y^2)} - \frac{r^2 C_0(r, t)}{4(\gamma^{-1}x^2 + \gamma y^2)} \quad (26) \\ &= \frac{1}{2\pi} \sum_{m'=-\infty}^{+\infty} e^{im'\phi'} (m' - r^2) C_0(r, t) \\ &\quad \times \int_0^{2\pi} \frac{e^{-im'\phi} d\phi}{4[\gamma r^2 + (\gamma^{-1} - \gamma)r^2 \cos^2 \phi]} \quad (27) \end{aligned}$$

Opening the $m = 0$ to $m' = 0$ channel enhances the $m = 0$ component transfer in the presence of the GP. If the $m = 0$ component dominates in the cylindrical wave expansion (CWE) Eq. (19), including the GP will significantly alter non-adiabatic dynamics.

To estimate the significance of the GP effect due to the $m = 0$ transfer enhancement we compute the CWE at the moment t_{CI} of the closest proximity of a wave-packet to the CI point. Once the coefficient $C_0(r, t_{\text{CI}})$ is found, we evaluate the average weight of the $m = 0$ component as

$$\bar{w} = \int r |C_0(r, t_{\text{CI}})|^2 dr. \quad (28)$$

If \bar{w} is much smaller than 50%, the $m = 0$ component is not dominant and including the GP will not produce significant change in nuclear dynamics.

Although \bar{w} contains all necessary information about the $m = 0$ component, dynamical simulations are required to compute it. However, for cases when the energy splitting (tuning) coordinate is strictly orthogonal to the coupling coordinate we can devise a simpler characteristic to assess the importance of the $m = 0$ GP effect without running simulations. For that we resort to a semiclassical consideration assuming a frozen Gaussian form of the nuclear wave function. Due to the orthogonality of the tuning and coupling coordinates the Franck-Condon (FC) point is shifted along the x coordinate. Hence the nuclear wave function will have a momentum $\mathbf{p} = (p_x, 0)$ upon arrival at the CI and the form

$$\Psi(x, y) = \sqrt{\frac{2}{\pi\sigma_x\sigma_y}} \exp\left(-\frac{x^2}{\sigma_x^2} - \frac{y^2}{\sigma_y^2}\right) \exp(-ip_x x). \quad (29)$$

Considering $|\Psi(x, y)|^2$ as the density of an ensemble of classical particles, each particle of this ensemble has an

absolute value of the classical angular momentum $|l_z| = |p_x y|$ with respect to the CI point. Using the relation between the momentum and kinetic energy $p_x^2/2 = E_{\text{kin}}$, and the estimate of E_{kin} as the difference between the potential energies of the wave-packet in the initial position $W_+(\mathbf{r}_{\text{ini}})$ and in the CI point $W_+(\mathbf{r}_{\text{CI}})$, we have

$$p_x = \sqrt{2[W_+(\mathbf{r}_{\text{ini}}) - W_+(\mathbf{r}_{\text{CI}})]}. \quad (30)$$

The angular momentum quantum number of the classical particle can be estimated as $m \approx |p_x y|$, so that a region $-r_{\text{eff}} < y < r_{\text{eff}}$, where

$$r_{\text{eff}} = p_x^{-1}. \quad (31)$$

corresponds to $|p_x y| < 1$ values and is assigned to the quantum value $m = 0$. Therefore, the average weight of the $m = 0$ component in Eq. (28) can be approximated as

$$\begin{aligned} \bar{w} &\approx \bar{w}_{\text{app}} = \int_{-\infty}^{\infty} dx \int_{-r_{\text{eff}}}^{r_{\text{eff}}} |\Psi(x, y)|^2 dy \\ &= \text{erf}\left(\frac{\sqrt{2}r_{\text{eff}}}{\sigma_x}\right) \quad (32) \end{aligned}$$

$$= \text{erf}\left(\frac{1}{\sigma_x \sqrt{W_+(\mathbf{r}_{\text{ini}}) - W_+(\mathbf{r}_{\text{CI}})}}\right). \quad (33)$$

Thus, evaluation of \bar{w}_{app} in Eq. (33) does not require dynamical simulations and uses only the σ_x parameter of the initial Gaussian and the adiabatic potential values $W_+(\mathbf{r}_{\text{ini}})$ and $W_+(\mathbf{r}_{\text{CI}})$.

C. Extension to N -dimensional LVC model

To extend our analysis to realistic molecular models we consider a general N -dimensional linear vibronic coupling model¹ with the Hamiltonian

$$\begin{aligned} \hat{H}_{\text{ND}} &= \sum_j \frac{1}{2} (p_j^2 + \omega_j^2 q_j^2) \mathbf{1}_2 + \begin{pmatrix} \kappa_j q_j & c_j q_j \\ c_j q_j & \tilde{\kappa}_j q_j \end{pmatrix} \\ &\quad + \begin{pmatrix} -\delta/2 & 0 \\ 0 & \delta/2 \end{pmatrix}, \quad (34) \end{aligned}$$

where q_j and p_j are mass-weighted coordinates and conjugated momenta, ω_j are frequencies, $\kappa_j, \tilde{\kappa}_j$, and c_j are linear coupling constants, and δ is the energy difference between the two diabatic electronic potentials in the FC point. As shown in previous studies⁴³⁻⁴⁵ the N -dimensional LVC model can adequately reproduce vibronic spectra of molecular systems with CIs. Another advantage of the N -dimensional LVC model is that its short time dynamics can be obtained from effective Hamiltonians of a lower dimensionality.⁴⁶⁻⁴⁸ There exist unitary transformations that rotate nuclear coordinates of H_{ND} so that after a truncation of all but a few collective DOF essential dynamical characteristics of H_{ND}

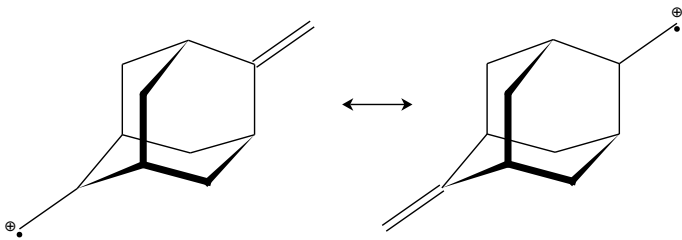


FIG. 2. The bis(methylene) adamantyl cation has two charge-localized conformation that are the result of a Jahn-Teller distortion from a symmetric configuration of the CI seam minimum.

(e.g., auto-correlation functions, electronic populations) can still be reproduced. In this work we use a reduction procedure that is similar in spirit to those used in Refs. 25, 46–48 but different in its focus on recovering a few lowest time derivatives of diabatic electronic populations of the full N -dimensional LVC Hamiltonian by its reduced counterpart. After the unitary rotation and truncation detailed in the Appendix we obtain the following effective 2D Hamiltonian

$$\hat{H}_{2D} = \left(\frac{P_X^2 + P_Y^2}{2} + \frac{\Omega_1^2 X^2 + \Omega_2^2 Y^2}{2} \right) \mathbf{1}_2 + \begin{pmatrix} \frac{1}{2}\Delta & \Delta_{12} \\ \Delta_{12} & -\frac{1}{2}\Delta \end{pmatrix} + \begin{pmatrix} D_1 X + D_2 Y & C_1 X + C_2 Y \\ C_1 X + C_2 Y & -D_1 X - D_2 Y \end{pmatrix}, \quad (35)$$

where X, Y and P_X, P_Y are collective coordinates and corresponding momenta, and $D_i, C_i, \Omega_i, \Delta, \Delta_{12}$ are constants defined in the Appendix. The Hamiltonian \hat{H}_{2D} [Eq. (35)] can be seen as the generalization of the 2D LVC Hamiltonian. Due to molecular symmetry all systems studied in this work have $C_1 = D_2 = \Delta_{12} = 0$ and thus, the 2D consideration can be extended directly to short-term dynamics of such N -dimensional systems.

III. NUMERICAL EXAMPLES

Here we consider three molecular systems with CIs that are well described by multi-dimensional LVC models: the bis(methylene) adamantyl (BMA)⁴⁹ (Fig. 2) and butatriene^{1,5,9,12,47,50} cations, and the pyrazine molecule.^{6,7,11,51} N -dimensional LVC models for these systems are taken from literature^{9,52,53}. Our dimensionality reduction procedure is applied to obtain parameters of 2D effective LVC Hamiltonians Eq. (1) (see Table I). To quantify GP effects we solve the time-dependent Schrödinger equation in a finite basis for three model Hamiltonians derived from the effective 2D LVC Hamiltonian: 1) the full Hamiltonian [Eq. (1)], 2) the “no GP” Hamiltonian [Eq. (6)], and 3) the “no GP, no DBOC” Hamiltonian [Eq. (18)]. For all three models we compare the adiabatic population dynamics $P_{\text{adi}}(t) = \langle \psi_{\text{adi}}^{(e)}(t) | \psi_{\text{adi}}^{(e)}(t) \rangle$, where $\psi_{\text{adi}}^{(e)}(x, y, t)$ is a time-dependent nuclear wave-function that corresponds to the excited

TABLE I. Parameters of the 2D effective LVC Hamiltonian, Eq. (1), for the studied systems.

ω_1	ω_2	a	c	Δ
Bis(methylene) adamantyl cation				
7.743×10^{-3}	6.680×10^{-3}	31.05	8.092×10^{-5}	0.00000
Butatriene cation				
9.557×10^{-3}	3.3515×10^{-3}	20.07	6.127×10^{-4}	0.01984
Pyrazine				
3.650×10^{-3}	4.186×10^{-3}	48.45	4.946×10^{-4}	0.02757

TABLE II. Parameters characterizing the importance of GP effects in the studied systems. The values have been obtained using 2D effective Hamiltonian parameters and Eqs. (5), (28), and (33).

γ	$ \gamma^{-1} - \gamma $	\bar{w} , %	\bar{w}_{app} , %
Bis(methylene) adamantyl cation			
0.09	11.4	42.2	42.1
Butatriene cation			
0.67	0.83	87.8	86.4
Pyrazine			
1.5	0.82	89.5	73.5

adiabatic electronic state. There are two sets of the initial conditions employed in this work: i) a wave-packet is taken as a Gaussian function Eq. (29) with widths $\sigma_x = \sqrt{2/\omega_1}$ and $\sigma_y = \sqrt{2/\omega_2}$ and ii) the same Gaussian function as in (i) but multiplied by the y coordinate. In both sets the initial position of a wave-packet is chosen at the FC point of the ground state of the corresponding full-dimensional models, and the initial momentum is set to zero. If the first set of initial conditions corresponds to a regular setup of an ultrafast laser photo experiment, the second setup has been designed to assess the importance of the GP effect associated with non-adiabatic transfer of the $m = 0$ component. Multiplication of the Gaussian function by y creates the nodal line $y = 0$ in the wave-packet and eliminates the $m = 0$ component from the corresponding CWE (19).

To connect the results of our numerical calculations to our theoretical analysis in Table II we present parameters that are most relevant to GP effects for all studied systems. Among other parameters we found it useful to characterize anisotropy of the DBOC by the absolute difference $|\gamma^{-1} - \gamma|$ that was inspired by the angular integral consideration in Eq. (25). For systems where the DBOC has cylindrical symmetry $|\gamma^{-1} - \gamma| = 0$, while deviation from the cylindrical symmetry increases $|\gamma^{-1} - \gamma|$.

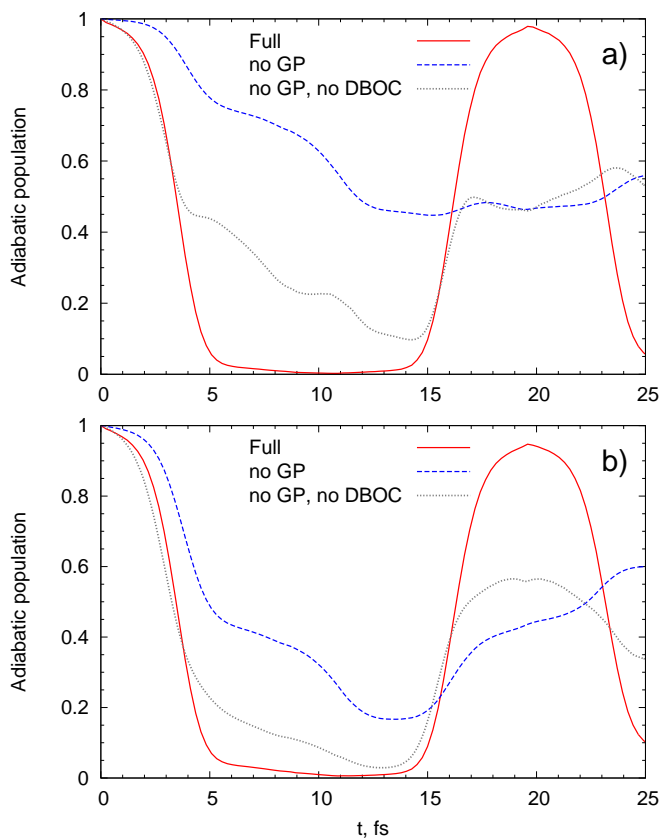


FIG. 3. Excited state population dynamics of the BMA cation with different initial wave-packets: a) Gaussian wave-packet (29), b) the same as (a) but multiplied by the coupling coordinate.

A. Bis(methylene) adamantyl cation

A high DBOC anisotropy for the BMA cation (Table II) suggests importance of GP effects via the DBOC compensation mechanism. As evident from the adiabatic population dynamics for all three models given in Fig. 3a this is indeed the case. The full model with the GP demonstrates the fastest initial population decay followed closely by the simplified model with no GP and no DBOC. The model without the GP (but with the DBOC) shows the slowest transfer since the wave-packet cannot reach a strong coupling region due to the DBOC repulsion.

Based on the average weight of the $m = 0$ component of the CWE [Eq. (19)] $\bar{w} = 42.2\%$ (see Table II), GP modification of the $m = 0$ transfer can play a role in deviation of the simplified model dynamics from that of the full model. Comparing dynamics without the $m = 0$ component (Fig. 3b) shows that even in this highly anisotropic case removing the $m = 0$ component visibly increases the overall transfer in the simplified model and makes it closer to the exact result.

The frozen Gaussian estimate of the $m = 0$ component weight $\bar{w}_{\text{app}} = 42.1\%$ is in excellent agreement with the exact value $\bar{w} = 42.2\%$. Due to a high energy excess

the wave-packet slides quickly along the tuning coordinate toward the CI point, preserving the Gaussian form. Thus, all assumptions made in the derivation of Eq. (33) are satisfied in this system.

A distinct feature of the full model is coherent oscillations of the adiabatic population. They can be easily understood considering the dynamics in the diabatic representation where, due to very weak linear couplings, the initial wave-packet oscillates coherently on a single diabatic potential. These oscillations result in the oscillatory adiabatic population dynamics because regions of the diabatic potential before and after an intersection region correspond to different adiabatic states. In the simplified (“no GP, no DBOC”) model the adiabatic population oscillations have similar frequency as in the full model but have quite different amplitude and more fine structural elements. The first CI passage dynamics is very similar in both models but the difference increases when the wave-packet reflected by the repulsive part of the ground state potential returns to the CI point. On this returning trajectory absence of the DBOC in the simplified model allows the wave-packet not only to transfer back to the excited state but also to pass through the CI point remaining on the ground adiabatic surface. Thus, in the simplified model, the wave-packet *bifurcates* at the CI, and this bifurcation gives rise to nuclear decoherence that damps the coherent oscillations.

B. Butatriene cation

The butatriene cation has a relatively low anisotropy of the DBOC (see Table II) and is not expected to exhibit large GP effects due to the DBOC compensation mechanism. Indeed, short-time adiabatic population dynamics (Fig. 4a) shows almost no difference between models with and without the DBOC, whereas dynamics in both models are quite different from that of the full model with the GP. The CWE according to Eq. (19) at the closest to the CI position, shows dominance of the $m = 0$ component with its average weight of $\bar{w} = 87.8\%$. Thus, as it is also seen from the dynamics with nodal initial Gaussian (Fig. 4b), a role of the GP for the butatriene cation is in facilitating transfer of the $m = 0$ component. Figure 4a illustrates that including the GP can reduce an initial population transfer time-scale in 2-3 times with respect to those of models without the GP.

The frozen Gaussian estimate of the $m = 0$ component weight ($\bar{w}_{\text{app}} = 86.4\%$) is in excellent agreement with the exact value due to spatial proximity of the initial FC position of the wave-packet and the CI point. The FC point, which corresponds to the ground-state minimum of the neutral molecule, is located only 8.8 a.u. apart from the CI point. The initial Gaussian distribution simply does not have time to change its shape appreciably.

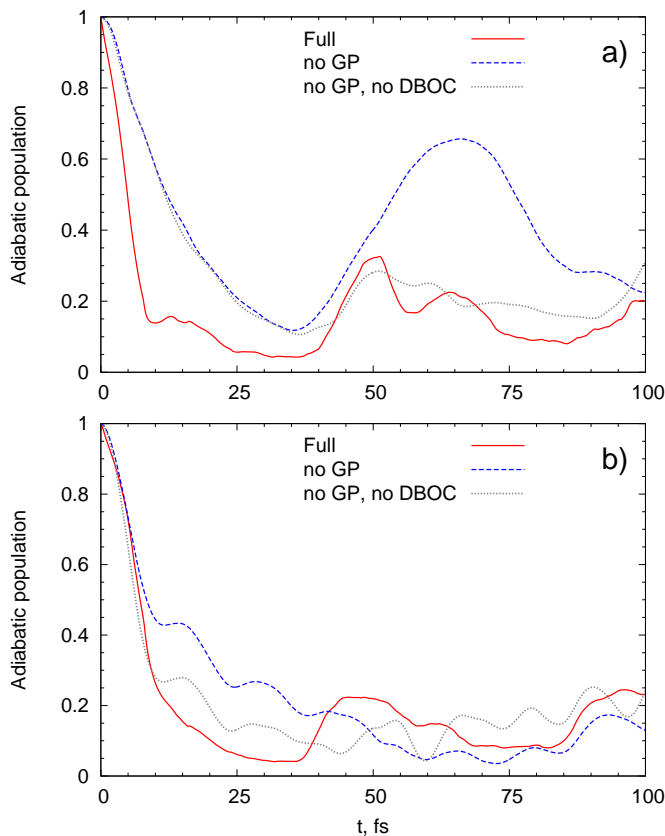


FIG. 4. Excited state population dynamics of $C_4H_4^+$ with different initial wave-packets: a) Gaussian wave-packet (29), b) the same as (a) but multiplied by the coupling coordinate.

C. Pyrazine molecule

Comparing parameters for pyrazine and the butatriene cation in Table II we find surprising similarity that should result in similar dynamical trends: relative insignificance of the DBOC compensation and dominance of the $m = 0$ transfer correction. Indeed, the excited state adiabatic population dynamics given in Fig. 5a confirms that the DBOC repulsion does *not* contribute much to the difference between models with and without the GP. Also, if we remove the $m = 0$ component from the initial wave-packet the adiabatic populations of all three models become similar (see Fig. 5b).

The only small difference between the pyrazine molecule and butatriene cation according to Table II is that the approximate weight of the $m = 0$ component for pyrazine has somewhat poorer agreement with its exact value. This deviation can be explained by a relatively long 48 a.u. spatial separation between the FC and CI points in pyrazine. The nuclear wave-packet does not go directly to the CI point and spends substantial time in other regions of space, changing the shape. Thus, the frozen Gaussian approximation is less accurate in this case.

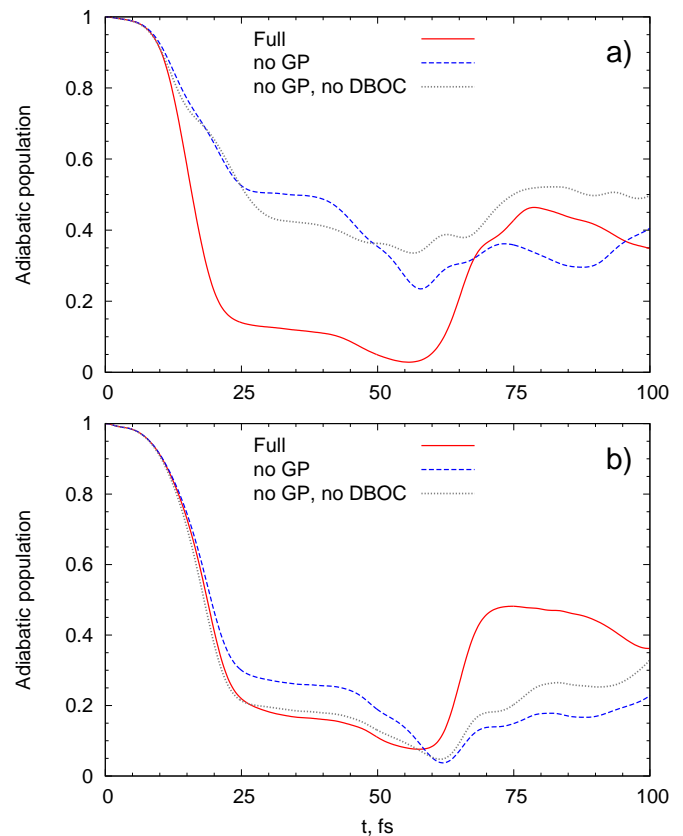


FIG. 5. Excited state population dynamics of pyrazine with different initial wave-packets: a) Gaussian wave-packet (29), b) the same as (a) but multiplied by the coupling coordinate.

IV. CONCLUDING REMARKS

Two cornerstones of our analysis of GP effects in radiationless transitions of molecular systems through CIs are the transformation of the N -dimensional LVC model to the effective 2D LVC model, and the local analysis of the latter in the adiabatic representation. For the effective 2D Hamiltonian the GP has been introduced by transforming the Hamiltonian with the Mead and Truhlar¹⁸ position-dependent phase factor.

Our local analysis revealed two main mechanisms of the GP contribution to non-adiabatic transitions. First, the GP compensates for repulsion caused by the DBOC, and second, it enhances transfer probability for a component of a nuclear wave-packet that corresponds to the zero eigenvalue of the L_z operator defined with respect to the CI point.

Two indicators have been introduced to quickly assess both GP effects: the anisotropy of the dimensionless coupling strength $|\gamma^{-1} - \gamma|$, and the weight \bar{w} of the $m = 0$ component in cylindrical wave expansion (19). The former can be readily calculated from parameters of the nuclear Hamiltonian, whereas the latter requires a dynamical simulation with the effective 2D Hamiltonian. Considering dynamics of a frozen Gaussian wave-packet with the assumption of orthogonality between coupling

and tuning modes we have proposed the estimate of \bar{w} [Eq. (33)] that can be evaluated without dynamical simulations but using only a wave-packet width and the potential energy difference between an initial and CI points.

Using numerical simulations of adiabatic population dynamics for the BMA and butatriene $C_4H_4^+$ cations and the pyrazine molecule, it is shown that the introduced indicators allow a reliable prediction of the GP role for studied systems. All systems exhibited substantial GP effects that can alter initial population transfer time-scales by factor of 2 to 3. Interestingly, GP effects in the studied systems modify non-adiabatic dynamics through different mechanisms. For the BMA cation the GP compensates for the DBOC repulsion, and for the butatriene cation and pyrazine molecule it strongly enhances non-adiabatic transition for the $m = 0$ component of an incident wave-packet.

All systems treated in this paper were chosen so that the N -dimensional LVC model would be adequate for them. An interesting question is whether our treatment can be extended to more general non-LVC Hamiltonians. Since the core of our analysis is the local consideration in the vicinity of a CI point we can claim that as long as a nuclear wave-function approaches the CI seam close enough for the LVC parametrization to be accurate our analysis will be adequate. To confirm these ideas through numerical simulations we plan to apply the developed analysis to non-LVC models of CIs in pyrrole.^{28,29}

Finally, in view of the DBOC compensating role of the GP it is clear why common approximations omitting the DBOC and GP contributions work quite well together in mixed quantum-classical non-adiabatic dynamics simulations. In addition, for non-adiabatic dynamics near the CI, adding the DBOC term should be accompanied by including the GP. Adding only the DBOC term without the GP in the best case will not affect dynamics appreciably but in the worst case can create uncompensated artificial repulsion and qualitatively incorrect dynamics. We hope that the proposed analysis will stimulate developments of new approximate methods for non-adiabatic dynamics in the adiabatic representation and will be of use in understanding results of simulations of non-adiabatic processes.

V. ACKNOWLEDGMENTS

A.F.I. thanks Paul Brumer for stimulating discussions and acknowledges funding from the Natural Sciences and Engineering Research Council of Canada (NSERC) through the Discovery Grants Program. L.J.D. is grateful to the European Union Seventh Framework Programme (FP7/2007-2013) for the financial support under grant agreement PEOF-GA-2012-332233.

Appendix: Effective reduced dimensional model

Below we describe the transformation from the N -dimensional LVC Hamiltonian [Eq. (34)] to the effective 2D Hamiltonian [Eq. (35)], and show that the reduced model can reproduce the short time population dynamics of the full model.

1. Reduction procedure

Recently, there has been significant progress in understanding how short time dynamics of the N -dimensional LVC model can be simulated using low dimensional Hamiltonians.^{46–48} Cederbaum and coworkers⁴⁷ have shown several approaches to building low dimensional effective Hamiltonians that reproduce short-time dynamic of the full Hamiltonian. The reason for this success was found comparing cumulant expansions of the auto-correlation functions of the effective and full Hamiltonians. With only three effective modes it is possible to construct an effective Hamiltonian that will reproduce three first cumulants of the total Hamiltonian. In our previous work on GP effects for low energy dynamics we developed a transformation similar to those proposed by Cederbaum and coworkers with the crucial difference that our transformation resulted in only a two dimensional subsystem.²⁵ In the current work the dynamical properties of our transformation have been improved by introducing a frequency weighting step. As shown below, this step creates better agreement between time derivatives of electronic population dynamics for the effective and full Hamiltonians.

a. Frequency weighting.— Starting with the N -dimensional LVC Hamiltonian [Eq. (34)] we modify its coordinates $\tilde{q}_j = \sqrt{\omega_j} q_j$ and momenta $\tilde{p}_j = p_j / \sqrt{\omega_j}$. The resulting Hamiltonian is

$$H_1 = \left[\frac{1}{2} (\tilde{\mathbf{p}}^\dagger \boldsymbol{\omega} \tilde{\mathbf{p}} + \tilde{\mathbf{q}}^\dagger \boldsymbol{\omega} \tilde{\mathbf{q}}) + \tilde{\mathbf{f}}^\dagger \tilde{\mathbf{q}} \right] \mathbf{1}_2 + \begin{pmatrix} \tilde{\mathbf{d}}^\dagger \tilde{\mathbf{q}} & \tilde{\mathbf{c}}^\dagger \tilde{\mathbf{q}} \\ \tilde{\mathbf{c}}^\dagger \tilde{\mathbf{q}} & -\tilde{\mathbf{d}}^\dagger \tilde{\mathbf{q}} \end{pmatrix} + \begin{pmatrix} \delta/2 & 0 \\ 0 & -\delta/2 \end{pmatrix}, \quad (\text{A.1})$$

where a vector notation is introduced: $\tilde{\mathbf{q}} = \{\tilde{q}_j\}_{j=1}^N$, $\tilde{\mathbf{p}} = \{\tilde{p}_j\}_{j=1}^N$, $\tilde{\mathbf{d}} = \{\frac{\kappa_j - \tilde{\kappa}_j}{2\sqrt{\omega_j}}\}_{j=1}^N$, $\tilde{\mathbf{f}} = \{\frac{\kappa_j + \tilde{\kappa}_j}{2\sqrt{\omega_j}}\}_{j=1}^N$, $\tilde{\mathbf{c}} = \{c_j / \sqrt{\omega_j}\}_{j=1}^N$, and $\boldsymbol{\omega} = \text{diag}\{\omega_1, \dots, \omega_N\}$ is a diagonal matrix of frequencies.

b. Definition of the effective coordinates.— To perform a truncation that would keep all non-adiabatic effects within a two-dimensional subspace we define a new set of coordinates $\{Q_1, Q_2, \dots, Q_N\}$ obtained from $\{\tilde{q}_1, \tilde{q}_2, \dots, \tilde{q}_N\}$ by an orthogonal transformation \mathbf{O}_1 : $\mathbf{Q} = \mathbf{O}_1 \tilde{\mathbf{q}}$. The first two rows of \mathbf{O}_1 define a 2D subsystem of the effective coordinates Q_1 and Q_2

$$\begin{pmatrix} \mathbf{e}_d^T \\ (\tilde{\mathbf{c}}^T - \tilde{C}_1 \mathbf{e}_d^T) / \tilde{C}_2 \end{pmatrix}, \quad (\text{A.2})$$

where

$$\begin{aligned} \mathbf{e}_d &= \tilde{\mathbf{d}} / \|\tilde{\mathbf{d}}\|, \\ \tilde{\mathbf{C}}_1 &= \tilde{\mathbf{c}} \cdot \mathbf{e}_d, \\ \tilde{\mathbf{C}}_2 &= \sqrt{\|\tilde{\mathbf{c}}\|^2 - (\tilde{\mathbf{c}} \cdot \mathbf{e}_d)^2}. \end{aligned} \quad (\text{A.3})$$

The remainder of \mathbf{O}_1 and coordinates $\{\tilde{Q}_j\}_{j=3}^N$ are defined by the Gram-Schmidt orthogonalization procedure with respect to the $\{\tilde{Q}_1, \tilde{Q}_2\}$ subspace. In the $\{\tilde{Q}_i\}$ representation the Hamiltonian becomes

$$\begin{aligned} H_2 &= \left[\frac{1}{2} (\tilde{\mathbf{P}}^\dagger \boldsymbol{\Lambda} \tilde{\mathbf{P}} + \tilde{\mathbf{Q}}^\dagger \boldsymbol{\Lambda} \tilde{\mathbf{Q}}) + \tilde{\mathbf{F}}^\dagger \tilde{\mathbf{Q}} \right] \mathbf{1}_2 + \begin{pmatrix} \delta/2 & 0 \\ 0 & -\delta/2 \end{pmatrix} \\ &+ \begin{pmatrix} \tilde{D}_1 \tilde{Q}_1 & \tilde{C}_1 \tilde{Q}_1 + \tilde{C}_2 \tilde{Q}_2 \\ \tilde{C}_1 \tilde{Q}_1 + \tilde{C}_2 \tilde{Q}_2 & -\tilde{D}_1 \tilde{Q}_1 \end{pmatrix}, \end{aligned} \quad (\text{A.4})$$

where $\boldsymbol{\Lambda} = \mathbf{O}_1 \boldsymbol{\omega} \mathbf{O}_1^\dagger$, $\tilde{\mathbf{F}} = \mathbf{O}_1 \tilde{\mathbf{f}}$, and $\tilde{D}_1 = \|\tilde{\mathbf{d}}\|$. A convenient feature of the H_2 Hamiltonian is that all differences between electronic surfaces and couplings are concentrated in the two-dimensional $\{\tilde{Q}_1, \tilde{Q}_2\}$ subspace. Next, we truncate the full set of coordinates $\tilde{\mathbf{Q}}_S = \begin{pmatrix} \tilde{Q}_1 \\ \tilde{Q}_2 \end{pmatrix} = \boldsymbol{\Pi} \tilde{\mathbf{Q}}$ and momenta $\tilde{\mathbf{P}}_S = \begin{pmatrix} \tilde{P}_1 \\ \tilde{P}_2 \end{pmatrix} = \boldsymbol{\Pi} \tilde{\mathbf{P}}$ to the two-dimensional subspace using a projector $\boldsymbol{\Pi}$. This truncation leads to the two-dimensional effective Hamiltonian

$$\begin{aligned} H_3 &= \left[\frac{1}{2} (\tilde{\mathbf{P}}_S^\dagger \boldsymbol{\Lambda}_S \tilde{\mathbf{P}}_S + \tilde{\mathbf{Q}}_S^\dagger \boldsymbol{\Lambda}_S \tilde{\mathbf{Q}}_S) + \tilde{\mathbf{F}}_S^\dagger \tilde{\mathbf{Q}}_S \right] \mathbf{1}_2 \\ &+ \begin{pmatrix} \tilde{\mathbf{D}}_S^\dagger \tilde{\mathbf{Q}}_S & \tilde{\mathbf{C}}_S^\dagger \tilde{\mathbf{Q}}_S \\ \tilde{\mathbf{C}}_S^\dagger \tilde{\mathbf{Q}}_S & -\tilde{\mathbf{D}}_S^\dagger \tilde{\mathbf{Q}}_S \end{pmatrix} + \begin{pmatrix} \delta/2 & 0 \\ 0 & -\delta/2 \end{pmatrix}. \end{aligned} \quad (\text{A.5})$$

All vectors and matrices are assigned the subscript S to indicate their two-dimensional character.

c. Extra transformations to the 2D LVC Hamiltonian.— To arrive at a subsystem Hamiltonian that is closer in form to the 2D LVC Hamiltonian [Eq. (1)] we diagonalize the frequency matrix $\boldsymbol{\Lambda}_S$ with the orthogonal transformation \mathbf{O}_2 , $\boldsymbol{\Omega} = \mathbf{O}_2 \boldsymbol{\Lambda}_S \mathbf{O}_2^\dagger$, and reverse the frequency weighting of coordinates. These transformations lead to new effective coordinates $\mathbf{Q} = \boldsymbol{\Omega}^{-\frac{1}{2}} \mathbf{O}_2 \tilde{\mathbf{Q}}_S$, momenta $\mathbf{P} = \boldsymbol{\Omega}^{\frac{1}{2}} \mathbf{O}_2 \tilde{\mathbf{P}}_S$, and the Hamiltonian

$$\begin{aligned} H_4 &= \left[\frac{1}{2} (\mathbf{P}^\dagger \mathbf{P} + \mathbf{Q}^\dagger \boldsymbol{\Omega}^2 \mathbf{Q}) + \mathbf{F}^\dagger \mathbf{Q} \right] \mathbf{1}_2 \\ &+ \begin{pmatrix} \mathbf{D}^\dagger \mathbf{Q} & \mathbf{C}^\dagger \mathbf{Q} \\ \mathbf{C}^\dagger \mathbf{Q} & -\mathbf{D}^\dagger \mathbf{Q} \end{pmatrix} + \begin{pmatrix} \delta/2 & 0 \\ 0 & -\delta/2 \end{pmatrix}, \end{aligned} \quad (\text{A.6})$$

where $\mathbf{F} = \boldsymbol{\Omega}^{\frac{1}{2}} \mathbf{O}_2 \tilde{\mathbf{F}}_S$, $\mathbf{D} = \boldsymbol{\Omega}^{\frac{1}{2}} \mathbf{O}_2 \tilde{\mathbf{D}}_S$, $\mathbf{C} = \boldsymbol{\Omega}^{\frac{1}{2}} \mathbf{O}_2 \tilde{\mathbf{C}}_S$. Finally, we translate the origin of the the 2D subspace $X = Q_1 + \Omega_1^{-2} F_1$, $Y = Q_2 + \Omega_2^{-2} F_2$ and obtain the Hamiltonian given in Eq. (35)

$$\begin{aligned} H_{2D} &= \left(\frac{P_X^2 + P_Y^2}{2} + \frac{\Omega_1^2 X^2 + \Omega_2^2 Y^2}{2} \right) \mathbf{1}_2 + \begin{pmatrix} \frac{\Delta}{2} & \Delta_{12} \\ \Delta_{12} & -\frac{\Delta}{2} \end{pmatrix} \\ &+ \begin{pmatrix} D_1 X + D_2 Y & C_1 X + C_2 Y \\ C_1 X + C_2 Y & -D_1 X - D_2 Y \end{pmatrix}, \end{aligned} \quad (\text{A.7})$$

where $\Delta = \delta - 2\mathbf{D}^\dagger \boldsymbol{\Omega}^{-2} \mathbf{F}$, and $\Delta_{12} = -\mathbf{C}^\dagger \boldsymbol{\Omega}^{-2} \mathbf{F}$. Note that the FC point, initially at the origin of the coordinate system in the N -dimensional space, is now shifted by the vector $\boldsymbol{\Omega}^{-2} \mathbf{F}$.

2. Short-time population dynamics

To assess the difference in short time population dynamics for the full [Eq. (A.4)] and reduced [Eq. (A.5)] models we compare low order terms of population Taylor time series for both models. However, due to a non-polynomial form of the adiabatic Hamiltonian [Eq. (6)], derivation of analytical expressions for adiabatic populations becomes intractable. To avoid this complication we focus on the *diabatic* population $P_{\text{dia}}(t)$:

$$P_{\text{dia}}(t) = \langle \Psi(0) | e^{i\hat{H}_{\text{dia}} t} \hat{P}_{\text{dia}} e^{-i\hat{H}_{\text{dia}} t} | \Psi(0) \rangle. \quad (\text{A.8})$$

Here, $\hat{P}_{\text{dia}} = \begin{pmatrix} 1 & 0 \\ 0 & 0 \end{pmatrix}$ is the projector to the diabatic state that has higher energy in the FC point, \hat{H}_{dia} is a general diabatic Hamiltonian that can be either H_2 or H_3 , and $|\Psi(0)\rangle$ is the initial total wave-function. We expand $P_{\text{dia}}(t)$ (A.8) in a Taylor series

$$P_{\text{dia}}(t) = \sum_{k=0}^{\infty} \frac{t^k}{k!} M_k \quad (\text{A.9})$$

where $M_k = d^k P_{\text{dia}}(t) / dt^k |_{t=0}$. First few terms of this expansion define short-time dynamics and for the reduced model to reproduce the full model dynamics, corresponding terms of two expansions should be close. Using Eq. (A.8) M_k 's can be alternatively defined as

$$M_k = i^k \sum_{l=0}^{l=k} \frac{(-1)^l k!}{l!(k-l)!} \langle \Psi(0) | \hat{H}_{\text{dia}}^{k-l} \hat{P}_{\text{dia}} \hat{H}_{\text{dia}}^l | \Psi(0) \rangle. \quad (\text{A.10})$$

Due to time reversal symmetry of the population dynamics at $t = 0$ all odd derivatives are zero. Using N -dimensional Gaussian wave-packet in the initial conditions $[\Psi(0) \propto (\exp\{-\tilde{\mathbf{Q}}^\dagger \tilde{\mathbf{Q}}/2\}, 0)^\dagger]$ and Gaussian integration the first three even orders of M_k for the N -dimensional Hamiltonian (A.4) are obtained

$$M_0 = 1, \quad (\text{A.11})$$

$$M_2 = -\tilde{\mathbf{C}}^\dagger \tilde{\mathbf{C}}, \quad (\text{A.12})$$

$$\begin{aligned} M_4 &= \tilde{\mathbf{C}}^\dagger (\boldsymbol{\Lambda} - \delta \mathbf{1}_N)^2 \tilde{\mathbf{C}} + 4 \left(\tilde{\mathbf{C}}^\dagger \tilde{\mathbf{D}} \right)^2 \\ &+ \tilde{\mathbf{C}}^\dagger \tilde{\mathbf{C}} \left(6\tilde{\mathbf{C}}^\dagger \tilde{\mathbf{C}} + 2\tilde{\mathbf{D}}^\dagger \tilde{\mathbf{D}} \right). \end{aligned} \quad (\text{A.13})$$

Corresponding terms for the reduced model [Eq. (A.5)] are evaluated similarly using the 2D Gaussian wave-

packet $\Psi(0) \propto (\exp\{-\tilde{\mathbf{Q}}_S^\dagger \tilde{\mathbf{Q}}_S/2\}, 0)^\dagger$

$$M_{0,S} = 1, \quad (\text{A.14})$$

$$M_{2,S} = -\tilde{\mathbf{C}}_S^\dagger \tilde{\mathbf{C}}_S, \quad (\text{A.15})$$

$$M_{4,S} = \tilde{\mathbf{C}}_S^\dagger (\mathbf{\Lambda}_S - \delta \mathbf{1}_2)^2 \tilde{\mathbf{C}}_S + 4 \left(\tilde{\mathbf{C}}_S^\dagger \tilde{\mathbf{D}}_S \right)^2 + \tilde{\mathbf{C}}_S^\dagger \tilde{\mathbf{C}}_S \left(6 \tilde{\mathbf{C}}_S^\dagger \tilde{\mathbf{C}}_S + 2 \tilde{\mathbf{D}}_S^\dagger \tilde{\mathbf{D}}_S \right). \quad (\text{A.16})$$

The zeroth-order terms are the same in both expansions, while relations between the corresponding second- and fourth-order terms need some elaboration. By construction of the orthogonal transformation \mathbf{O}_1 [Eq. (A.2)], $\tilde{\mathbf{D}}$ and $\tilde{\mathbf{C}}$ have $N - 2$ zero entries: $\tilde{C}_j = \tilde{D}_j = 0$, $j = 3, \dots, N$. Therefore, we have the following identity

$$\tilde{\mathbf{C}}^\dagger \tilde{\mathbf{C}} = \tilde{\mathbf{C}}^\dagger \mathbf{\Pi} \tilde{\mathbf{C}} = \tilde{\mathbf{C}}_S^\dagger \tilde{\mathbf{C}}_S \quad (\text{A.17})$$

which proves that $M_{2,S} = M_2$. Similarly, all terms of M_4 but $\tilde{\mathbf{C}}^\dagger \mathbf{\Lambda}^2 \tilde{\mathbf{C}}$ coincide with corresponding terms of $M_{4,S}$. Generally we have

$$\begin{aligned} \tilde{\mathbf{C}}^\dagger \mathbf{\Lambda}^2 \tilde{\mathbf{C}} &= \tilde{\mathbf{C}}^\dagger \mathbf{\Pi} \mathbf{\Lambda}^2 \mathbf{\Pi} \tilde{\mathbf{C}} = \tilde{\mathbf{C}}_S^\dagger \mathbf{\Lambda}^2 \tilde{\mathbf{C}}_S \\ &\neq \tilde{\mathbf{C}}_S^\dagger \mathbf{\Lambda}_S^2 \tilde{\mathbf{C}}_S = \tilde{\mathbf{C}}_S^\dagger (\mathbf{\Pi} \mathbf{\Lambda} \mathbf{\Pi})^2 \tilde{\mathbf{C}}_S, \end{aligned} \quad (\text{A.18})$$

where the inequality is due to the existence of couplings between the two-dimensional subspace and the complementary space in $\mathbf{\Lambda}$. In the BMA case, the relative error in M_4 due to the inequality turns out to be small $(M_4 - M_{4,S})/M_4 = 8 \cdot 10^{-3}$. Moreover, for the butatriene cation and the pyrazine molecule, because the $\tilde{\mathbf{c}}$ vector in Eq. (A.1) contains only a single non-zero component the transformations from H_1 to H_3 leave $\tilde{\mathbf{C}}_S$ decoupled from the other coordinates. Therefore, for these systems, the inequality in Eq. (A.18) becomes an equality and $M_4 = M_{4,S}$.

Comparison of diabatic populations obtained with the full and reduced models are shown in Fig. 6. To simulate dynamics in the full dimensional diabatic models we used the MCTDH package.⁵⁴ For all systems there is a very good agreement between results of the full and reduced model dynamics until the end of the first CI passage: 15 fs for BMA (see Fig. 3), 35 fs for the butatriene cation (see Fig. 4), and 45 fs for the pyrazine molecule (see Fig. 5). Similar trends we see for the adiabatic populations in Fig. 7, and thus we can conclude that the mode reducing transformation preserves the short-time non-adiabatics dynamics in the studied systems very well.

¹H. Köppel, W. Domcke, and L. S. Cederbaum, "Multimode Molecular Dynamics Beyond the Born-Oppenheimer Approximation," (John Wiley & Sons, Inc., 1984) Chap. 2, pp. 59–246.

²D. R. Yarkony, *Rev. Mod. Phys.* **68**, 985 (1996).

³S. Hahn and G. Stock, *J. Phys. Chem. B* **104**, 1146 (2000).

⁴B. Balzer, S. Hahn, and G. Stock, *Chem. Phys. Lett.* **379**, 351 (2003).

⁵L. Cederbaum, W. Domcke, H. Köppel, and W. Von Niessen, *Chem. Phys.* **26**, 169 (1977).

⁶L. Seidner, W. Domcke, and W. von Niessen, *Chem. Phys. Lett.* **205**, 117 (1993).

⁷C. Woywod, W. Domcke, A. L. Sobolewski, and H.-J. Werner, *J. Chem. Phys.* **100**, 1400 (1994).

⁸B. Kendrick and R. T. Pack, *J. Chem. Phys.* **104**, 7502 (1996).

⁹C. Cattarius, G. A. Worth, H.-D. Meyer, and L. S. Cederbaum, *J. Chem. Phys.* **115**, 2088 (2001).

¹⁰V. Vallet, Z. Lan, S. Mahapatra, A. L. Sobolewski, and W. Domcke, *J. Chem. Phys.* **123**, 144307 (2005).

¹¹I. Burghardt, K. Giri, and G. A. Worth, *J. Chem. Phys.* **129**, 174104 (2008).

¹²S. Sardar, A. K. Paul, P. Mondal, B. Sarkar, and S. Adhikari, *Phys. Chem. Chem. Phys.* **10**, 6388 (2008).

¹³A. Sirjoosingh and S. Hammes-Schiffer, *J. Chem. Theory Comput.* **7**, 2831 (2011).

¹⁴W. Domcke and D. R. Yarkony, *Annu. Rev. Phys. Chem.* **63**, 325 (2012).

¹⁵G. J. Halász, M. Šindelka, N. Moiseyev, L. S. Cederbaum, and Á. Vibók, *J. Phys. Chem. A* **116**, 2636 (2012).

¹⁶Q. Ou and J. E. Subotnik, *J. Phys. Chem. C* **117**, 19839 (2013).

¹⁷M. V. Berry, *Proc. R. Soc. A* **392**, 45 (1984).

¹⁸C. A. Mead and D. G. Truhlar, *J. Chem. Phys.* **70**, 2284 (1979).

¹⁹M. V. Berry, *Proc. R. Soc. A* **414**, 31 (1987).

²⁰H. C. Longuet-Higgins, U. Opik, M. H. L. Pryce, and R. A. Sack, *Proc. R. Soc. A* **244**, 1 (1958).

²¹D. Babikov, B. K. Kendrick, P. Zhang, and K. Morokuma, *The Journal of Chemical Physics* **122**, 044315 (2005).

²²D. Babikov and B. K. Kendrick, *The Journal of Chemical Physics* **133**, 174310 (2010).

²³J. Schön and H. Köppel, *J. Chem. Phys.* **103**, 9292 (1995).

²⁴I. G. Ryabinkin and A. F. Izmaylov, *Phys. Rev. Lett.* **111**, 220406 (2013), arXiv:1306.6387v2.

²⁵L. Joubert-Doriol, I. G. Ryabinkin, and A. F. Izmaylov, *J. Chem. Phys.* **139**, 234103 (2013), arXiv:1310.2929.

²⁶J. C. Juanes-Marcos, S. C. Althorpe, and E. Wrede, *Science* **309**, 1227 (2005).

²⁷S. C. Althorpe, *J. Chem. Phys.* **124**, 084105 (2006).

²⁸S. C. Althorpe, T. Stecher, and F. Bouakline, *J. Chem. Phys.* **129**, 214117 (2008).

²⁹F. Bouakline, *Chem. Phys.* (2014), 10.1016/j.chemphys.2014.02.010.

³⁰H. A. Jahn and E. Teller, *Proc. R. Soc. Lond. A* **161**, 220 (1937).

³¹I. B. Bersuker, *Chem. Rev.* **101**, 1067 (2001).

³²M. S. Child, in *The Role of degenerate States in Chemistry*, Advances in Chemical Physics, Vol. 124, edited by M. Baer and G. D. Billing (John Wiley & Sons, Inc., 2003) pp. 1–38.

³³F. T. Smith, *Phys. Rev.* **179**, 111 (1969).

³⁴M. Baer, *Chem. Phys. Lett.* **35**, 112 (1975).

³⁵C. A. Mead, *J. Chem. Phys.* **77**, 6090 (1982).

³⁶H. Köppel and B. Schubert, *Mol. Phys.* **104**, 1069 (2006).

³⁷T. Van Voorhis, T. Kowalczyk, B. Kaduk, L.-P. Wang, C.-L. Cheng, and Q. Wu, *Ann. Rev. Phys. Chem.* **61**, 149 (2010).

³⁸D. R. Yarkony, *Chem. Rev.* **112**, 481 (2012).

³⁹J. E. Subotnik, R. J. Cave, R. P. Steele, and N. Shenoi, *J. Chem. Phys.* **130**, 234102 (2009).

⁴⁰We need to specify the direction of action of L_z because L_z does not commute with the denominator $(x^2 + \gamma^2 y^2)$ unless $\gamma = 1$.

⁴¹N. C. Handy and A. M. Lee, *Chem. Phys. Lett.* **252**, 425 (1996).

⁴²E. F. Valeev and C. D. Sherrill, *J. Chem. Phys.* **118**, 3921 (2003).

⁴³Q. Meng and H.-D. Meyer, *J. Chem. Phys.* **138**, 014313 (2013).

⁴⁴Z. Li, M. E.-A. Madjet, and O. Vendrell, *J. Chem. Phys.* **138**, 094313 (2013).

⁴⁵C. Lévesque, A. Komainda, R. Taïeb, and H. Köppel, *J. Chem. Phys.* **138**, 044320 (2013).

⁴⁶L. Cederbaum, E. Gindensperger, and I. Burghardt, *Phys. Rev. Lett.* **94**, 113003 (2005).

⁴⁷I. Burghardt, E. Gindensperger, and L. S. Cederbaum, *Mol. Phys.* **104**, 1081 (2006).

⁴⁸E. Gindensperger, I. Burghardt, and L. S. Cederbaum, *J. Chem. Phys.* **124**, 144103 (2006).

⁴⁹L. Blancafort, P. Hunt, and M. A. Robb, *J. Am. Chem. Soc.* **127**, 3391 (2005).

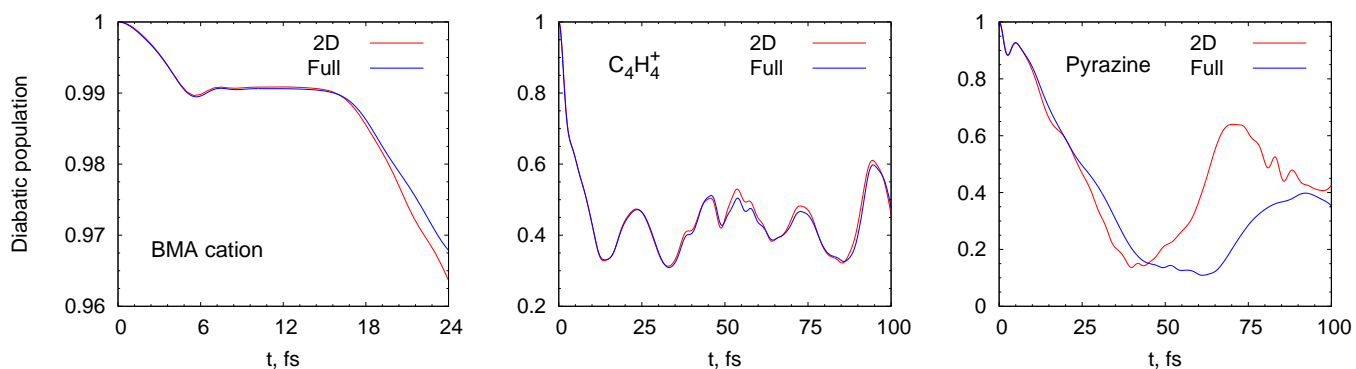


FIG. 6. Diabatic population dynamics for the full and effective two-dimensional models.

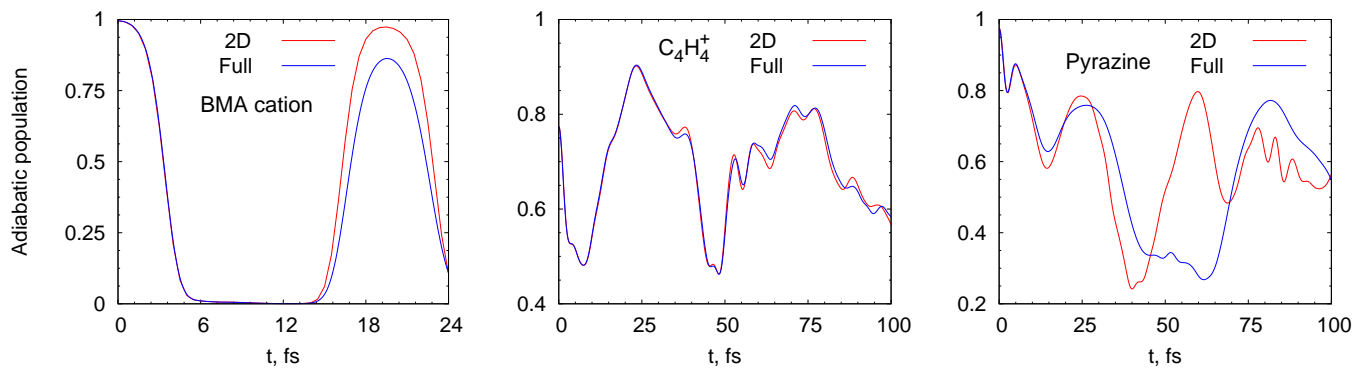


FIG. 7. Adiabatic population dynamics for the full and effective two-dimensional models.

⁵⁰E. Gindensperger, I. Burghardt, and L. S. Cederbaum, *J. Chem. Phys.* **124**, 144104 (2006).

⁵¹M. Sukharev and T. Seideman, *Phys. Rev. A* **71**, 012509 (2005).

⁵²A. F. Izmaylov, D. Mendive-Tapia, M. J. Bearpark, M. A. Robb, J. C. Tully, and M. J. Frisch, *J. Chem. Phys.* **135**, 234106 (2011).

⁵³A. Raab, G. A. Worth, H.-D. Meyer, and L. S. Cederbaum, *J. Chem. Phys.* **110**, 936 (1999).

⁵⁴G. A. Worth, M. H. Beck, A. Jackle, and H.-D. Meyer, "MCTDH development version 9.0".